Hydrol. Earth Syst. Sci. Discuss., 3, 2385–2436, 2006
www.hydrol-earth-syst-sci-discuss.net/3/2385/2006/
© Author(s) 2006. This work is licensed
under a Creative Commons License.

Hydrology and Earth System Sciences Discussions

Papers published in *Hydrology and Earth System Sciences Discussions* are under open-access review for the journal *Hydrology and Earth System Sciences*

Uncertainties in rainfall retrievals from ground-based weather radar: overview, case study, and simulation experiment

R. Uijlenhoet[1], S. H. van der Wielen[1], and A. Berne[2]

[1]Hydrology and Quantitative Water Management Group, Department of Environmental Sciences, Wageningen University, The Netherlands
[2]Laboratoire d'étude des Transferts en Hydrologie et Environnement (LTHE), Grenoble, France

Received: 13 July 2006 – Accepted: 17 July 2006 – Published: 28 August 2006

Correspondence to: R. Uijlenhoet (Remko.Uijlenhoet@wur.nl)

Abstract

Because rainfall constitutes the main source of water for the terrestrial hydrological processes, accurate and reliable measurement and prediction of its spatial and temporal distribution over a wide range of scales is an important goal for hydrology. We investigate the potential of ground-based weather radar to provide such measurements through a detailed analysis of the associated observation uncertainties. First, a historical perspective on measuring the space-time distribution of rainfall, from the rain gauge to the radar era, is presented. Subsequently, we provide an overview of the various errors and uncertainties affecting radar rainfall retrievals. As an example, we present a case study of the relation between measurements from an operational C-band weather radar and a network of tipping bucket rain gauges as a function of range. Finally, a recently developed stochastic model of range profiles of rainfall microstructure is employed in a simulation experiment designed to investigate the rainfall retrieval uncertainties associated with weather radars operating in different widely used frequency bands.

1 Introduction

Accurate and reliable measurement and prediction of the spatial and temporal distribution of rainfall over a wide range of scales is an important goal for hydrology, because rainfall constitutes the main source of water for the terrestrial hydrological processes. Ground-based weather radars are in principle well-suited to provide such measurements because: (1) they cover extended areas while measuring from a single point; (2) they allow rapid access for real-time hydrological applications; (3) their spatial and temporal resolution is generally higher than what can be obtained using rain gauge networks (see Fig. 1).

However, radar is a remote sensing technique, which implies that weather radars measure the electromagnetic properties of rain in the air, rather than the distribution

HESSD

3, 2385–2436, 2006

of rain rates at the ground which is needed for hydrological applications. The conversion of the radar reflectivities measured aloft to rain rates at the ground constitutes the observer's problem in radar hydrometeorology. Both the reflectivity measurements themselves and the radar reflectivity – rain rate conversion are prone to errors and uncertainties. Quantification of the observation uncertainties associated with rainfall retrievals from ground-based weather radars is a prerequisite for the assimilation of radar-retrieved rainfall fields in hydrological models and constitutes the main topic of this paper.

Section 2 provides a historical perspective on measuring the space-time distribution of rainfall, from the rain gauge to the radar era. Section 3 gives an overview of the various errors and uncertainties affecting radar rainfall retrievals. A case study of radar – rain gauge comparison is presented in Sect. 4. In Sect. 5 we discuss a simulation experiment designed to investigate the rainfall retrieval uncertainties associated with weather radars operating in different widely used radio frequency bands. Finally, Sect. 6 presents the main conclusions of this paper.

2 Rainfall measurement: a historical perspective

2.1 The rain gauge era

Traditionally, information on the atmospheric component of the hydrological cycle has been gathered from rain gauges. A basic problem with rain gauges, however, is the fact that they represent point measurements. This means that their limited spatial representativeness can only be increased indirectly, through temporal accumulation. Even then, the spatial representativeness of rain gauges remains unclear, as it will depend on the dynamics of the rainfall process under consideration. Moreover, accumulation of rain gauge measurements reduces their ability to capture the temporal structure of rainfall. This trade-off between spatial representativeness and temporal resolution is a fundamental problem associated with rain gauges. Additional difficulties are related to

HESSD
3, 2385–2436, 2006

all kinds of practical issues associated for instance with wind effects and maintenance (e.g. Neff, 1977; Sevruk, 1989; Habib et al., 1999; Steiner et al., 1999).

The application of rain gauges in networks has long been considered a solution to the problem. All kinds of procedures have been proposed over the years to interpolate spatially between the rain gauges and fill in the gaps. However, the density of the network (in the form of the mean inter-gauge distance), together with the dynamical properties of the rainfall process (its spatial structure and characteristic advection velocity), dictate a lower limit to the temporal resolution of the spatially interpolated rain gauge measurements. The result is that, from a hydrological point of view, many operational rain gauge networks are too sparse to provide information on the rainfall process at a satisfactory spatial and temporal resolution (e.g. Berne et al., 2004). Denser networks, on the other hand, would generally be very impractical (and more expensive than most people think).

An additional problem is that even the most sophisticated spatial interpolation procedures (such as the geostatistical technique known as kriging) generally lack the ability to capture the extreme rainfall variability found in nature. The interpolated rainfall fields are simply too smooth (e.g. Wood et al., 2000). Incidentally, the same holds for rainfall fields simulated by many of the stochastic point process models proposed over the years for modeling the phenomenology of rainfall at the ground (e.g. Le Cam, 1961; Waymire and Gupta, 1981a,b,c; Smith and Karr, 1983; Rodríguez-Iturbe et al., 1984, 1986, 1987, 1988; Waymire et al., 1984; Smith and Karr, 1985; Rodríguez-Iturbe, 1986; Rodríguez-Iturbe and Eagleson, 1987; Smith, 1987). Recent advances in (multi)fractal descriptions of rainfall fields (e.g. Rodríguez-Iturbe et al., 1989; Lovejoy and Schertzer, 1990a,b, 1995; Rodríguez-Iturbe, 1991; Georgakakos et al., 1994; Veneziano et al., 2006; Venugopal et al., 2006) may provide opportunities in this direction, although they will never be able to overcome the fundamental shortcomings of rain gauges.

2.2 Weather radar

The remote sensing of rainfall using ground-based radar is a technology which has been in continuous development since World War II. It is currently reaching a state of maturity which renders its hydrological application feasible (e.g. Collier, 1993; Smith et al., 1996b; Ogden et al., 1999; Sempere Torres et al., 1999; Borga, 2002; Berne et al., 2005b; Delrieu et al., 2005; Berenguer et al., 2005). Radars can provide complete spatial and temporal coverage of an area from one single measurement site and as such they are in principle well suited to hydrological applications.

RADAR is the acronym for "RAdio Detection And Ranging". According to Battan (1973), radar can be defined as "the art of detecting by means of radio echoes the presence of objects, determining their direction and range, recognizing their character and employing the data thus obtained". The principle of radar remote sensing is based upon the transmission of a coded radio signal, the reception of a backscattered signal from the volume of interest and inferring the properties of the objects contained in that volume by comparing the transmitted and received signals. In the case of radar meteorology, the objects in the scattering volume are in principle hydrometeors (precipitation particles), although occasionally the ground surface may be detected as well. Hydrometeors can be raindrops, but snow flakes and ice crystals as well. The main interest from a hydrological perspective lies obviously in the raindrops.

Already since the early 1970s, attempts have been made to use weather radar to estimate the spatial and temporal distribution of rainfall for hydrological applications (e.g. Battan, 1973; CHO-TNO, 1977). For almost three decades, radar has been a promise to hydrology. A promise however, which until recently has not been possible to keep. This has been due to both the material and the methods used at the time. First of all, most weather radars which have been used for hydrological applications until recently, were part of existing meteorological radar networks. These instruments were not designed with the hydrological application in mind. For instance, their spatial and temporal resolutions and sampling capabilities were generally insufficient. Secondly,

the manner in which the radar data were used was generally not suited to the problem at hand. The hydrologists who were tackling the problem at the time did not pay attention to the principle of radar measurements.

During the 1980s, all kinds of more or less sophisticated statistical schemes were devised to combine the information from radars with that from networks of rain gauges, the type of information hydrologists were used to working with (e.g. Collier, 1986a,b; Collier and Knowles, 1986; Krajewski, 1987; Creutin et al., 1988; Delrieu et al., 1988; Azimi-Zonooz et al., 1989; Seo et al., 1990a,b; Seo and Smith, 1991a,b; Smith, 1993). The idea was that rain gauges were providing the "ground truth" at various points in the area of interest. The radar data were then used in a sense to interpolate between the rain gauges. However, it remains to be seen to what extent rain gauges represent the truth, as "ground truth is the amount of rain that would have reached the ground if the rain gauge had not been there". Moreover, the lack of attention for the principle of radar measurements proved to work counter-productive. After adjustment of the radar data using the rain gauge measurements (erroneously called "calibration" at the time), all kinds of errors and inconsistencies remained which this approach was not able to solve.

2.3 Radar hydrology

Since the early 1990s, hydrologists working on the problem of radar rainfall estimation have begun to take a different, more physically-based approach. They are revisiting the established theory of weather radar developed in the 1950s and 1960s by their meteorological and radar engineering colleagues. However, this is done using today's radar technology and, moreover, from a hydrological perspective. The objective is to apply ground-based weather radar to estimate the spatial and temporal distribution of rainfall at the ground.

As opposed to the largely statistical approach of the 1980s, the current physical approach considers the principle of radar measurements and the microstructure of rainfall in quite some detail. Another new aspect is that rain gauges are no longer used

to "calibrate" the radar images, but mainly for verification purposes. This new approach, now beginning to be known as radar hydrology, is currently starting to provide its first results (e.g. Smith et al., 1996a,b; Andrieu et al., 1997; Creutin et al., 1997; Serrar et al., 2000; Sánchez-Diezma et al., 2000; Berne et al., 2005a; Delrieu et al., 2005; Berenguer et al., 2005). Weather radar is finally starting to redeem the promise it has been to hydrology for almost three decades.

3 Radar rainfall estimation: an overview

3.1 An inverse problem

Because radar is a remote sensing technique, it does not provide direct measurements of rainfall, but only indirect ones via the interaction with electromagnetic waves. Radar is a so-called active microwave technique, in which a radio signal with known properties (amplitude, frequency and polarization state) is sent into the scattering medium. In this case, the scattering medium is considered to be rainfall and the scatterers are raindrops. Part of the radio signal received by the raindrops is scattered back into the direction of the radar and received by its antenna. This is visualized in Fig. 2.

The difference between the properties of the transmitted and the received signal provides information on the dielectric properties of the scattering medium. It is the objective of radar hydrology to devise accurate and reliable methods ('retrieval algorithms') to convert this information into rainfall rates at the ground for hydrological applications. This so-called observer's problem is generally tackled in two main steps (e.g. Smith and Krajewski, 1993): (1) conversion of the reflectivity measured in the atmosphere to surface reflectivity; (2) conversion of surface reflectivity to rain rate. The exact manner in which these conversions are carried out will obviously affect the precision of the obtained radar rainfall estimates.

In order to be able to perform the conversion of the scattering properties of rainfall in the air into rainfall rates at the ground, some model of the microstructure of rainfall

and its interaction with the radar signal has to be used (e.g. Uijlenhoet et al., 1999b; Uijlenhoet and Sempere Torres, 2006). Since rainfall consists of individual raindrops with different sizes and hence different scattering properties, such a model should necessarily comprise a parameterization of the raindrop size distribution (e.g. Uijlenhoet and Stricker, 1999; Jameson and Kostinski, 2001). The model should be simple, however, as one should be able to invert it on the basis of radar measurements. More specifically, the number of model parameters should not exceed the number of variables estimated ("measured") by the radar system in question. Otherwise, the inversion problem would be under-determined. The algorithms used to invert the model and estimate the model parameters on the basis of the available radar measurements are known as retrieval algorithms.

Conventional weather radars are able to estimate only one property of the backscattered signal, namely its mean power. This mean power is commonly expressed in terms of a so-called radar reflectivity factor Z. The inversion model to be used with such one-parameter radar systems is therefore necessarily a one-parameter model. The classical Z–R model provides a direct relationship between the radar reflectivity factor Z and the rainfall rate R (e.g. Uijlenhoet, 2001). It has been common practice for more than half a century now (e.g. Marshall and Palmer, 1948) to take for this conversion a simple power-law relationship between Z and R. Because in reality there is much more uncertainty than what can be captured in this one-parameter model, the Z–R model is necessarily statistical in nature – it is a regression model (e.g. Haddad and Rosenfeld, 1997).

Establishing Z–R relationships has captured the attention of radar meteorologists since the early days of weather radar more than five decades ago. From the point of view of instrumentation, there exist two approaches. Such relationships are either calibrated in real time using simultaneous observations from a radar and a network of rain gauges (e.g. Wilson and Brandes, 1979) or determined in advance on the basis of observations of raindrop size spectra obtained from disdrometers or optical spectrometers (e.g. Marshall and Palmer, 1948). In both cases it is, apart from errors directly

related to the operation of the radar, the limited representativeness of the surface rainfall observations which affects the precision of the radar estimates of rainfall.

In an ideal situation, i.e. one in which all other possible error sources would be negligible, the main uncertainty in rainfall estimates by (conventional, i.e. single parameter) weather radar would be due to uncertainty in the Z–R relationship. In practice, this would mean a situation where a non-attenuated, pencil beam weather radar is observing nearby homogeneous rainfall close to the ground. In reality, these requirements are hardly ever met. Therefore, in any practical situation the uncertainty in the Z–R relationship will provide a lower bound to the uncertainties associated with radar rainfall estimation.

Over the past years, operational ground-based weather radars have become capable of measuring, apart from the mean power, the Doppler and polarization properties of the backscattered signal as well. These multi-parameter radar systems have created the possibility of using inversion models with more than one parameter. Such models are able to capture more aspects of the microstructure of rainfall than the simple Z–R model. It is the hope that with such models, a larger fraction of the uncertainty is captured and that, as a result, the rainfall estimates become more reliable. The development of retrieval algorithms for multi-parameter radar systems is currently receiving a lot of attention (e.g. Illingworth et al., 2000; Testud et al., 2000; Vulpiani et al., 2005, 2006).

3.2 Sources of uncertainty

Up to this point, we have assumed that radars are able to measure the scattering properties of rainfall perfectly and that, as a consequence, the only remaining problem is the conversion of these properties to rainfall rates at the ground. This would imply that uncertainty in the raindrop size distribution would be the main error source. Nothing is less true, however. A series of additional problems remains to be tackled before the objective of radar hydrology can be considered achieved.

Perhaps the most fundamental problem of all is that of calibration. If a radar system

is not well calibrated, then the measured powers do not correspond to the actual powers. This will introduce a bias in the radar power measurements which greatly affects the corresponding rainfall estimates. Hence, for hydrological applications, it is very important to have a well-calibrated radar system and to control its stability over time (e.g. Atlas, 2002).

Additional problems associated with the quantitative use of weather radar can be more easily appreciated if the geometrical configuration of radar measurements is considered in some more detail. Although the radar antenna can in principle be pointed in any direction, the greatest spatial coverage can of course be obtained if it is used in a rotating fashion at a low elevation angle. This is the preferred configuration for operational meteorological and hydrological applications. In this configuration, the radar is providing the user with circular images with fixed resolutions in distance ("range" in radar terminology) and angle. An example of such a "Plan Position Indicator" (PPI) can be found in Fig. 1.

Although any subdivision of additional problems associated with the quantitative use of weather radar is necessarily arbitrary, we have made an attempt by identifying two classes of problems: (1) instrumental effects, i.e. effects associated purely with the principle of radar measurement; (2) environmental effects, i.e. effects associated with the interaction of the radar signal with its environment (the atmosphere and the ground).

3.2.1 Instrumental effects

A first instrumental effect in weather radar measurements is the range effect caused by the spatial expansion of the radar beam. This expansion, associated with the radar's fixed angular resolution, has the effect that the spatial resolution of the radar, both in the horizontal and in the vertical, decreases with range. Hence, the further away from the radar, the worse the spatial variability of the rainfall field is captured. Figure 3 shows the range dependence of the diameter and the 1 km deep sample volume of the Royal Netherlands Meteorological Institute (KNMI) weather radar.

An extreme example of this occurs when, at appreciable distances from the radar

(say 100 km), the volume of the resolution cells increases to the extent (of the order of a km^3) where situations of partial beam filling may occur. Unless corrected for, this may lead to serious underestimations of radar reflectivities and the corresponding rain rates (e.g. Joss and Waldvogel, 1990; Durden et al., 1998).

Apart from its spatial expansion, it should be recognized that the weighting of the scatterers inside the radar beam is not done uniformly, neither in range nor in angle. In range, this non-uniform weighting is such that the center of a range resolution cell receives more weight than the front or tail ends. In angle, the radar beam consists of a main lobe with several side lobes. Again, the center of the resolution cell receives the heaviest weight. In conclusion, the reflectivity associated with a particular resolution cell is the convolution of the true spatial variability of the rainfall field at the cell's location with the radar's range and angular weighting functions. An example of the distribution of power along the center of the radar beam is given in Fig. 4.

An additional range effect can be associated with the fact that, even if the elevation angle of the radar is 0° (horizontal), the height of the beam axis increases with range due to the curvature of the earth. Hence, the further away from the radar, the less representative the measurements are for rain rates at ground level. A graphical representation of the propagation of the beam for the lowest elevation angle employed by the KNMI is presented in Fig. 5.

A particular example of this range effect is the problem of beam overshooting. In this case, the radar beam completely overshoots the precipitation area of interest. Close to the radar, such range effects can be partially compensated for by constructing a so-called "(pseudo-) Constant Altitude Plan Position Indicator" (pseudo-CAPPI). The principle of its construction is presented in Fig. 6. It is clear that at longer distances from the radar (exceeding 100 km), where even the lowest elevation angle of the radar exceeds the representative height of the CAPPI, this approach will not be able to fully compensate for range effects.

3.2.2 Environmental effects

The first environmental effect to be discussed here could just as well have been grouped under the instrumental effects in the previous section. It is the range effect associated with the attenuation of the radar signal as it propagates through the atmosphere, particularly at shorter wavelengths. Part of the radiation transmitted by the radar is absorbed or scattered (part of which back to the radar antenna) by the constituents of the atmosphere. Only a fraction of the total energy flux remains propagating away from the antenna. The problem with attenuation is that it is caused to a large extent by the very phenomenon radar hydrologists are interested in, rainfall itself. This renders attenuation a highly nonlinear effect which it is troublesome to correct for (e.g. Hitschfeld and Bordan, 1954; Marzoug and Amayenc, 1994; Berne and Uijlenhoet, 2005, 2006). This topic will be dealt with in greater detail in Sect. 5.

Other environmental effects are associated with the vertical structure of the atmosphere. For radar meteorological and hydrological purposes this vertical structure is often summarized in terms of a so-called vertical profile of reflectivity, the vertical profile of the radar reflectivity factor Z (e.g. Sánchez-Diezma et al., 2000; Berne et al., 2005a). An example of this VPR is presented in Fig. 7. Because melting snowflakes are seen by conventional (single parameter) weather radars as huge raindrops, the melting layer of precipitation (characteristic of stratiform conditions) causes a bright band on the radar screen (Fig. 8).

The problem with the vertical profile of reflectivity is that it is very difficult to correct for, because its actual structure at any location is unknown. It can have a strong spatial and temporal variability. Moreover, it generally causes a range effect due to the spatial expansion of the radar beam and its increasing height with range (e.g. Andrieu and Creutin, 1995; Andrieu et al., 1995).

Even in the absence of precipitation (i.e. in clear air), the vertical structure of the atmosphere may influence the performance of radar systems. During favorable meteorological conditions (particularly temperature and water vapor inversions), the vertical

profile of the refractive index of the atmosphere may be such that the electromagnetic waves transmitted by a radar are bent towards the earth's surface. In that case, we speak of anomalous propagation, or simply anaprop. As a result of anaprop, at some distance the radar signal will hit the earth's surface and cause so-called ground clutter. Large errors in rain rate estimates result if these clutters are erroneously interpreted as rainfall (e.g. Pamment and Conway, 1998).

Finally, it may be the earth's surface itself which causes problems. We have already encountered ground clutter as a result of anaprop. However, in mountainous terrain, ground clutter may even occur during standard propagation conditions. At the same time, the relief may cause partial or complete obstruction of the radar beam. Recent research has shown that, under particular conditions, ground clutter caused by relief may be used to estimate total attenuation and to test the stability of the radar calibration. This is one of the few occasions where it is advantageous to use radars in mountainous terrain (e.g. Serrar et al., 2000). Additional aspects of the assumptions, errors and uncertainties associated with radar rainfall retrievals are discussed among others by Battan (1973); Wilson and Brandes (1979); Sauvageot (1982); Doviak (1983); Zawadzki (1984); Clift (1985); Austin (1987); Collier (1989); Joss and Waldvogel (1990); Jameson (1991); Andrieu et al. (1997); Creutin et al. (1997); Sánchez-Diezma et al. (2001).

4 Radar – rain gauge comparison: an example

As an example of the comparison between weather radar-retrieved and rain gauge-measured rain rates, let us consider the event that occurred on 19 September 2001 in the southwestern part of The Netherlands. The month of September 2001 was the second wettest month ever recorded in The Netherlands. The KNMI in De Bilt measured a monthly sum of 210.7 mm, the record of 213.2 mm being measured in 1957. In many places monthly rainfall depths of more than 200 mm were recorded. Most rain fell in the southwestern part of The Netherlands, where, for instance, in Hoek van Holland

289 mm of rain were recorded, which is about 35% of the average total yearly rainfall. Of this amount 107 mm were recorded on the 19 September. Over a significant fraction of the province of Zuid-Holland more than 50 mm was recorded on that day. The rainfall event that occurred on 19 September can be characterized by a frontal (stratiform) weather situation with widespread rainfall. The center of the rain storm remained more or less stationary above the southwestern part of The Netherlands for several hours, causing inundations in the Hoogheemraadschap van Delfland and other water boards.

The available radar data consisted of 15-min volume scans from the operational C-band weather radar of the KNMI in De Bilt (Fig. 9), containing reflectivities up to 320 km at 14 different elevation angles ranging from 0.3 to 12.0 degrees. The reflectivities were averaged per radar range cell with a resolution of approximately 1 degree by 1 km.

Rain rates were measured using the KNMI weather station network of 35 automatic tipping bucket rain gauges located at 32 different sites in The Netherlands (Fig. 9). The gauge data were averaged to 10-min accumulations and converted to intensities in mm h^{-1}, assuming that the measured rain intensities remained constant during each 10-min period.

Radar and rain gauge data were compared on the basis of 30-min time intervals. To this end the reflectivity-derived rain rates of two 15-min interval radar volume scans were averaged and in a similar manner the rain rates from three 10-min gauge intervals were averaged. Figure 10 shows a comparison of the radar-derived reflectivities and the rain gauge-derived rain rates for three different range intervals. The range effects discussed previously are clearly visible. Note for instance the increased bias and scatter at longer ranges.

The underestimation of the radar-derived reflectivities with respect to the standard Marshall-Palmer Z–R relationship (which is considered to be representative for stratiform rainfall) may have been caused by attenuation of the radar signal while propagating through the rainfall event. The vertical profile of reflectivity and signal attenuation are probably the most important sources of error and uncertainty affecting rainfall retrievals from operational weather radars in flatland areas such as The Netherlands.

5 Simulation experiment

In this section a recently developed stochastic model of range profiles of rainfall microstructure is employed to perform controlled simulation experiments designed to investigate the rainfall retrieval uncertainties associated with weather radars operating in different widely used frequency bands. As noted in the previous section, many operational radar networks across Europe operate at relatively short wavelengths (C-band, ~5 cm), which may be severely attenuated in heavy rainfall. In addition, there has recently been an increased interest in high-resolution radars operating at even shorter wavelengths (X-band, ~3 cm), in particular for urban hydrological applications. Such X-band radars are much less expensive than C-band radars, mainly due to the smaller antennas needed to achieve the same angular resolution. Hence, there is potential for the application of such radar systems in relatively dense networks (e.g. CASA, http://www.casa.umass.edu). Quantitative radar rainfall estimation at X- and C-band is seriously hampered by attenuation of the radar signal by precipitation along its path, as has been recognized for a long time (e.g. Atlas and Banks, 1951). Therefore, the adverse effects of attenuation on radar-retrieved rainfall fields need to be identified and corrected for operationally.

We have developed a stochastic simulator of range profiles of raindrop size distributions (DSD), which provides a controlled experiment framework to investigate the accuracy and robustness of various attenuation correction algorithms (Berne and Uijlenhoet, 2005). This simulator was recently employed to quantify the influence of uncertainties concerning radar calibration, parameterization of the power-law relation between the radar reflectivity Z and specific attenuation k, and total path-integrated attenuation (PIA) estimates (Berne and Uijlenhoet, 2006). Here we focus on the uncertainty in the retrieved rainfall profiles from simulated single frequency, incoherent and non-polarimetric radar systems operating at X-, C- and S-band (~10 cm) associated with the spatial variability of rainfall (and the corresponding DSD) on scales between 25 m and 50 km. S-band is used as a reference against which to compare the other two

frequencies, because the former is known to be virtually immune to attenuation. This work complements previous experimental results concerning the uncertainty associated with attenuation correction due to the spatial variability of the DSD along a range profile (e.g. Delrieu et al., 1999), by posing the problem in a Monte Carlo framework.

5.1 Stochastic rainfall range profile simulator

The stochastic model of range profiles of raindrop size distributions used for the controlled simulation experiments described later in this section has been proposed by Berne and Uijlenhoet (2005). The description of the model largely follows that of Berne and Uijlenhoet (2006); it is summarized here for the sake of completeness. The model assumes that the local drop size distribution (DSD) can be described adequately by an exponential DSD, with two parameters N_t (total drop concentration) and Λ (inverse of a characteristic diameter) that are considered to be random variables:

$$N(D|N_t, \Lambda) = N_t \Lambda e^{-\Lambda D}, \quad (1)$$

where $N(D|N_t, \Lambda)dD$ denotes the drop concentration in the diameter interval $[D, D+dD]$ given N_t and Λ. The latter are assumed to be jointly lognormally distributed. A plausible spatial correlation structure is introduced in the range profiles by assuming $N' = \ln N_t$ and $\Lambda' = \ln \Lambda$ to follow a first order discrete vector auto-regressive process (e.g. Bras and Rodríguez-Iturbe, 1985):

$$\mathbf{X}[j+1] = \mathbf{C_1}\mathbf{C_0}^{-1}\mathbf{X}[j] + \mathbf{E}[j+1], \quad (2)$$

with

$$\mathbf{X}[j] = \begin{bmatrix} N'(j) - \mu_{N'} \\ \Lambda'(j) - \mu_{\Lambda'} \end{bmatrix} ,$$

$$\mathbf{C_0} = \begin{bmatrix} \sigma^2_{N'} & \sigma_{N'}\sigma_{\Lambda'}\rho_{N'\Lambda'} \\ \sigma_{N'}\sigma_{\Lambda'}\rho_{N'\Lambda'} & \sigma^2_{\Lambda'} \end{bmatrix} ,$$

$$\mathbf{C_1} = \begin{bmatrix} \sigma^2_{N'}\rho_{N'}(1) & \sigma_{N'}\sigma_{\Lambda'}\rho_{N'\Lambda'}(1) \\ \sigma_{N'}\sigma_{\Lambda'}\rho_{\Lambda'N'}(1) & \sigma^2_{\Lambda'}\rho_{\Lambda'}(1) \end{bmatrix} ,$$

$$\mathbf{E}[j+1] = \begin{bmatrix} \epsilon_{N'}(j+1) \\ \epsilon_{\Lambda'}(j+1) \end{bmatrix} ,$$

where j is the distance index, $\rho_{N'}(1)$ the auto-correlation at lag 1 (idem for Λ'), $\rho_{N'\Lambda'}(1)$ the cross-correlation at lag 1, and $\epsilon_{N'}$ a Gaussian white noise process (idem for Λ'). Hence, $\mathbf{C_0}$ and $\mathbf{C_1}$ represent the covariance matrices at lags 0 and 1, respectively. The variances of the white noise processes $\epsilon_{N'}$ and $\epsilon_{\Lambda'}$ are determined such that $\mathbf{X}$ is a second order stationary stochastic process. For a first order vector auto-regressive process, the auto-correlation functions are exponential:

$$\rho(r) = e^{-2r/\theta} , \tag{3}$$

where r denotes the distance lag and θ the characteristic spatial scale, also known as the scale of fluctuation (Vanmarcke, 1983):

$$\theta = 2 \int_0^\infty \rho(r)\, dr . \tag{4}$$

According to Eq. (3), θ essentially represents the decorrelation distance, i.e. the distance lag where the autocorrelation of the process has decreased to e^{-2}.

5.2 Model parameterization

The stochastic model described above allows the repeated generation of range profiles of DSDs of equivolumetric spherical raindrops. The model is parameterized using measurements of DSD time series collected with an optical spectropluviometer during the HIRE'98 experiment in Marseille, France (Uijlenhoet et al., 1999a). We have determined two sets of model parameters, a "moderate" rainfall parameterization for which we used the entire (3 h) rain event that occurred on 7 September 1998, and an "intense" rainfall parameterization that was fitted on a period of 45 min of high-intensity rainfall during the same event. Taylor's hypothesis with a constant velocity of 12.5 m s^{-1}, consistent with the wind speed estimate of Berne et al. (2004) is invoked to convert the measured DSD time series to DSD range profiles.

Both for the moderate and for the intense rainfall parameterization the zero-lag cross-correlations between the fitted N' and Λ' values are found to be negligible. Moreover, the scales of fluctuation θ for N' and Λ' are very close and will be assumed equal in what follows (although this is not a requirement of the model). The total number of model parameters has now reduced to five: the mean and standard deviation of N' and Λ', and the scale of fluctuation θ. Their values are given in Table 1, for both parameterizations.

In order to simulate the radar rainfall retrieval process over hydrologically relevant scales, we generate DSD profiles with a total length of 50 km for the moderate rainfall parameterization and 30 km for the intense parameterization. The spatial resolution for the moderate rainfall parameterization is taken to be 50 m (corresponding to a 4-s time step) and that for the intense parameterization 25 m (i.e. a 2-s time step).

5.3 Profiles of bulk rainfall variables

The radar equation relates the received power to the properties of the radar, those of the target (i.e. raindrops) and the distance (range) between radar and target. At attenuating wavelengths (such as X- and C-band) the classical radar equation (e.g.

Uijlenhoet, 2001) should be multiplied by an exponential factor accounting for the attenuation of the received signal due to rainfall present on the path between the radar antenna and the target (e.g. Battan, 1973):

$$\overline{P_r} = C\frac{|K|^2}{r^2}Z_A(r)\,, \tag{5}$$

with

$$Z_A(r) = Z(r)\exp\left[-c\int_0^r k(s)\,ds\right]\,, \tag{6}$$

where $\overline{P_r}$ [W] is the mean power received from raindrops at range r, C is the so-called radar constant (which is a function of the employed wavelength and antenna size, among other things), $|K|^2$ is a coefficient related to the dielectric constant of water ($\approx$0.93), Z_A [mm^6 m^{-3}] is the attenuated radar reflectivity factor, Z [mm^6 m^{-3}] is the actual radar reflectivity factor (simply called "radar reflectivity" from now on), k [dB km^{-1}] is the specific (one-way) attenuation coefficient (called "specific attenuation" hereafter), and c=0.2 ln(10).

All three bulk rainfall variables relevant for radar rainfall retrieval using incoherent, single frequency, non-polarimetric radar systems, namely Z, k and the rain rate R [mm h^{-1}], are (weighted) integrals over the raindrop size distribution. The radar reflectivity Z [mm^6 m^{-3}] is defined as

$$Z = \frac{10^6\lambda^4}{\pi^5|K|^2}\int_0^\infty \sigma_B(D)N(D|N_t,\Lambda)\,dD\,, \tag{7}$$

where λ [cm] denotes the wavelength of the radar signal and σ_B [cm^2] is the backscattering cross-section. Similarly, the specific one-way attenuation k [dB km^{-1}] is defined

as

$$k = \frac{1}{\ln 10} \int_0^\infty \sigma_E(D) N(D|N_t, \Lambda)\, dD\,, \tag{8}$$

where σ_E [cm^2] is the extinction cross-section. Finally, the rain rate R [mm h^{-1}] is defined as

$$R = 6\pi \times 10^{-4} \int_0^\infty D^3 v(D) N(D|N_t, \Lambda)\, dD\,, \tag{9}$$

where v [m s^{-1}] is the raindrop terminal fall velocity in still air. Using the Mie scattering theory for spherical particles (van de Hulst, 1981) to calculate the scattering cross-sections σ_B and σ_E and Beard's parameterization (Beard, 1976) to calculate the drop terminal fall speeds, profiles of the bulk rainfall variables Z, k and R are easily derived from the DSD profiles generated using the stochastic simulator described above.

Examples of generated radar reflectivity profiles for both rainfall parameterizations are shown in Fig. 11. The stochastic simulation model described above allows controlled experiments in a Monte Carlo framework to quantify the rainfall retrieval uncertainty associated with spatial rainfall variability for weather radar systems operating in different widely used frequency bands.

5.4 Rainfall retrieval algorithms

For incoherent, single frequency, non-polarimetric radar systems the observers's problem of radar hydrometeorology consists of solving the inverse problem posed by Eq. (6). This implies inverting Eq. (6), i.e. reconstructing the range profile of Z given that of Z_A, and subsequently converting the retrieved Z-profile to a rain rate (R) profile. Clearly, this inverse problem is ill-posed as long as no constraints on the relationships

between the bulk rain variables Z, k and R are specified. In accordance with all previous investigations in this field, we postulate the power-law relationships

$$Z = \alpha R^{\beta} = \gamma k^{\delta} \ . \tag{10}$$

We study two widely used attenuation correction algorithms. The first (Hitschfeld and Bordan, 1954) is based on the assumption that the measured reflectivity in the first range bin (i.e. the one closest to the radar) is not affected by attenuation. Using an a priori power-law relation between radar reflectivity and specific attenuation (Eq. 10), the path-integrated attenuation affecting the second range bin is calculated. Subsequently, the measured reflectivity in the second range bin is corrected and, using the same power-law relation, the path-integrated attenuation the third range bin is suffering is calculated and corrected for. In this manner an iterative correction for attenuation is carried out in the direction from the radar antenna towards the region of interest. Therefore this type of algorithm is termed "forward". Hitschfeld and Bordan (1954) (HB hereafter) derived a closed-form analytical solution to this problem in the limit where the radar range resolution tends to zero, reformulated here to express the retrieved (attenuation-corrected) rain rate (R') in terms of the measured (attenuated) reflectivities (Z_A):

$$R'(r) = \frac{\left(Z_A(r)/\alpha\right)^{1/\beta}}{\left[1 - \frac{c}{\delta}\int_0^r \left(\frac{Z_A(s)}{\gamma}\right)^{1/\delta} ds\right]^{\delta/\beta}} \ . \tag{11}$$

The fact that the integral is between 0 and r shows that the HB algorithm is a forward algorithm. Note that the difference in the denominator of Eq. (11) can reach values close to 0. This renders the HB algorithm potentially highly unstable (Hitschfeld and Bordan, 1954).

The second attenuation correction algorithm considered here has been developed to avoid such instability problems. It is based on the assumption that the path-integrated

attenuation (PIA) to a certain fixed target (e.g. a building or a mountain) at a given range r_0 is known. In practice the attenuation to this target can be estimated for instance by comparing the reflectivity of the target before and during a rainfall event. In this case the same iterative attenuation correction procedure is employed but this time in the direction from the fixed target towards the radar antenna. Therefore this type of algorithm is often referred to as "backward". Marzoug and Amayenc (1994) (MA hereafter) presented the corresponding analytical solution, reformulated here to express the retrieved (attenuation-corrected) rain rate (R') in terms of the measured (attenuated) reflectivities (Z_A):

$$R'(r) = \frac{\left(Z_A(r)/\alpha\right)^{1/\beta}}{\left[A_0^{1/\delta} + \frac{c}{\delta}\int_r^{r_0}\left(\frac{Z_A(s)}{\gamma}\right)^{1/\delta} ds\right]^{\delta/\beta}}, \quad (12)$$

where $A_0=A(r_0)$ equals the exponential factor in Eq. (6) evaluated at the range $r=r_0$, accounting for the (two-way) PIA between the radar antenna and the reference target.

The fact that the integral in Eq. (12) goes from r to r_0 (with $r_0>r$) shows that the MA algorithm is a backward algorithm. Also note that the minus sign in the denominator of Eq. (11) has now become a plus sign. Therefore, this type of algorithm is numerically stable by definition. The only disadvantage of backward algorithms with respect to forward algorithms is that they require reliable PIA estimates at ranges beyond the region of (hydrological) interest. In practice, such reference targets may not be available in all directions. Delrieu et al. (1997) were the first to apply this algorithm, which was originally developed for correcting (vertical) spaceborne radar rainfall profiles, to correct (horizontal) ground-based radar rainfall profiles.

5.5 Resulting uncertainties in radar rainfall retrievals

The uncertainty associated with radar rainfall retrievals based on the two attenuation correction algorithms presented above is studied in a Monte Carlo framework. We

focus on three frequency bands that are widely used operationally: X-band (3.2 cm wavelength), C-band (5.6 cm), and S-band (10.0 cm). The latter is used as a reference, because it is known that attenuation is negligible at S-band for all but the most extreme rainfall. We generate one thousand profiles of N_t and Λ and calculate from those (using Eqs. 7–9) the corresponding profiles of the bulk rainfall variables Z, k, Z_A), and R. To mimic the typical sampling resolutions of operational radar systems, the high spatial resolution (25 m, 50 m) profiles are averaged at a lower spatial resolution of 500 m. Table 2 lists some statistics of the generated profiles of the bulk rainfall variables Z, k, and R.

In previous attenuation correction sensitivity studies using the stochastic DSD range profile simulator (Berne and Uijlenhoet, 2005, 2006), we fitted a Z–k power-law relation on each profile separately using a non-linear regression technique. These relations necessarily constituted the best possible power-law relations for the generated profiles. This approach was adopted because we wanted to study the sensitivity of attenuation correction schemes to spatial rainfall variability (Berne and Uijlenhoet, 2005) and other sources of uncertainty (Berne and Uijlenhoet, 2006) per se. Here we approach the radar rainfall retrieval problem from an operational perspective. In practice, it would never be possible to have real-time estimates of the coefficients of the power-law Z–k and Z–R relations needed for radar rainfall retrieval at attenuating wavelengths, unless a network of instruments for measuring raindrop size distributions (disdrometers) would be deployed under the radar umbrella. This would not be feasible from an operational and financial perspective. Therefore, we employ climatological power-law Z–k and Z–R relations, whose coefficients α, β, γ, and δ (Eq. 10) are estimated following the procedure outlined by Delrieu et al. (1999), using a large dataset of DSD measurements collected in southern France (Table 3).

For the MA algorithm, we calculate the PIA value for each of the generated profiles (corresponding to A_0 in Eq. 12) as the difference between the non-attenuated and the attenuated Z values at the final range bin. In other words, we assume the PIA estimates to be exact (the effect of an error in the PIA estimates on the accuracy of the

MA algorithm was studied by Berne and Uijlenhoet, 2005, 2006).

We have applied the two attenuation correction algorithms (Eqs. 11 and 12) to the 1000 Z_A profiles using the climatological Z–k and Z–R relations. Because for hydrological applications the retrieved rain rate profiles are more relevant than the retrieved reflectivity profiles, we concentrate here on the former - the latter have been dealt with in previous work (Berne and Uijlenhoet, 2005, 2006). For each of the 1000 generated profiles, we have calculated two statistics quantifying the accuracy and uncertainty associated with the radar rainfall retrievals: the mean bias error (MBE) and the root mean square error (RMSE) between the retrieved and the actual rain rate profiles. Figures 12–15 show the 10%, 50% (median), and 90% quantiles of these statistics as a function of the profile-average rain rate for the three frequency bands and the two rainfall parameterizations considered.

For the moderate rainfall parameterization (Figs. 12 and 13), the path-average rain rates (over 50 km profiles) are found to vary between a few and almost 20 mm h^{-1}. The (backward) MA algorithm significantly outperforms the (forward) HB algorithm only at X-band frequencies for such moderate rain rates (Figs. 12 and 13, top panels). At C-band and even more prominently at S-band, the differences between the two attenuation correction algorithms are insignificant, given the appreciable amount of uncertainty associated with both error statistics caused by the statistical variability among the generated rainfall profiles within the moderate rainfall climatology. Moreover, the HB algorithm does not significantly diverge for any of the frequencies in case of moderate rain rates ("div"=0% on all occasions), not even at X-band, where the path-integrated attenuation is expected to be strongest.

Interestingly, the biases are almost always negative for the moderate rainfall parameterization, indicating that neither attenuation correction algorithm is fully able to compensate for the loss of power and reconstitute the true rain rate profiles. At X-band, the biases for the HB algorithm increase from about 20% of the path-average rain rate at 5 mm h^{-1} to more than 50% for path-average rain rates above 15 mm h^{-1} (Fig. 12, top panel). Therefore, even at moderate rain rates where numerical instabilities do not

HESSD
3, 2385–2436, 2006

seem to play a major role, the HB algorithm should be applied with great care at X-band. At C- and S-band, on the other hand, the biases tend to be limited to 15–20% of the path-average rain rate for both attenuation correction algorithms. Surprisingly, Fig. 12 (bottom panel) shows that even S-band radar signals in moderate rainfall tend to suffer from attenuation which cannot be fully corrected for. Of course, one has to keep in mind that path-integrated attenuation is a function of both path-average rain rate (and the associated rain rate variability along the path) and the path length, which in this case is relatively large (50 km). In addition, the derived climatological Z–k and Z–R relations may be less appropriate at this frequency for the moderate rainfall parameterization.

Although the general picture for the intense rainfall parameterization (Figs. 14 and 15) seems to be the same, the detailed results differ appreciably from those for the moderate rainfall parameterization. First of all, at X-band frequencies the HB attenuation correction algorithm now diverges in approximately one out of every four cases (24% of the profiles are numerically unstable). In addition, the bias remaining after attenuation correction using the HB algorithm exceeds 70% of the path-average rain rate for the most intense rainfall profiles, indicating a recovered fraction of the path-average rain rate of less than 30%. This clearly shows the complete failure of the HB algorithm for rain rate retrieval in intense rainfall at X-band, which is in accordance with previous results (e.g. Hitschfeld and Bordan, 1954; Delrieu et al., 1999; Berne and Uijlenhoet, 2005, 2006).

The MA algorithm, on the other hand, is able to correct almost entirely for the suffered signal loss at X-band on average, perhaps even better than for the moderate rainfall parameterization (Fig. 14, top panel). One should bear in mind, however, that the total path length in this case is only 30 km, as opposed to 50 km for the moderate rainfall parameterization. Moreover, the uncertainty associated with the retrieved rain rate profiles, as quantified by the RMSE in Fig. 15 (top panel) is appreciable for the most intense rainfall profiles, also for the MA algorithm. Interestingly, at C-band the MA algorithm seems to have a tendency to overcompensate for attenuation, which may

be caused by the fact that the employed climatological Z–k and Z–R relations are less appropriate at this frequency. At S-band, finally, both rainfall retrieval algorithms provide satisfactory results, although at this frequency the loss of power due to rain-induced attenuation is obviously not going to be a major source of error and uncertainty in the first place.

6 Conclusions

We have presented a detailed analysis of the observation uncertainties associated with rainfall estimates from ground-based weather radar. Rainfall being the main source of water for the terrestrial hydrological processes, accurate and reliable measurement and prediction of its space-time distribution over a wide range of scales is an important goal for hydrology.

First, a historical perspective on measuring the space-time distribution of rainfall, emphasising the development from rain gauge networks to weather radar, has been presented. Subsequently, we have provided an overview of the various errors and uncertainties affecting radar rainfall retrievals, both of an instrumental and of an environmental nature. We argue that accurate and reliable rainfall measurement using ground-based weather radar is only possible after a thorough physically-based treatment of the associated errors and uncertainties. As an example, we present a case study of the range-dependence of the relation between measurements from an operational C-band weather radar and a network of tipping bucket rain gauges. We show that quantitative precipitation estimation using operational weather radars at ranges beyond 100 km is problematic, even in relatively flat areas such as The Netherlands which are in principle well-suited for radar rainfall estimation.

Finally, the rainfall retrieval uncertainties associated with weather radars operating in different widely used frequency bands has been investigated using a recently developed stochastic simulation model of range profiles of rainfall microstructure. A detailed comparison between two different attenuation correction schemes, both in moderate

and in intense rainfall, shows that backward correction algorithms are more stable and accurate than forward algorithms, provided reliable estimates of the total path-integrated attenuation are available.

Acknowledgements. The work reported in this paper has been supported financially by EU Integrated Project FLOODsite (GOCE-CT-2004-505420). This paper reflects the authors' views and not those of the European Community. Neither the European Community nor any member of the FLOODsite consortium is liable for any use of the information in this paper. The first author acknowledges the Netherlands Organization for Scientific Research (NWO) for a grant (016.021.003) in the framework of the Innovational Research Incentives Scheme (Vernieuwingsimpuls). The weather radar and rain gauge data employed in this paper were kindly provided to us by I. Holleman of KNMI.

References

Andrieu, H. and Creutin, J.-D.: Identification of vertical profiles of radar reflectivity for hydrological applications using an inverse method. Part I: Formulation, J. Appl. Meteorol., 34, 225–239, 1995. 2396

Andrieu, H., Delrieu, G., and Creutin, J.-D.: Identification of vertical profiles of radar reflectivity for hydrological applications using an inverse method. Part II: Sensitivity analysis and case study, J. Appl. Meteorol., 34, 240–259, 1995. 2396

Andrieu, H., Creutin, J.-D., Delrieu, G., and Faure, D.: Use of a weather radar for the hydrology of a mountainous area. Part I: Radar measurement interpretation, J. Hydrol., 193, 1–25, 1997. 2391, 2397

Atlas, D.: Radar calibration – Some simple approaches, Bull. Amer. Meteorol. Soc., 83, 1313–1316, 2002. 2394

Atlas, D. and Banks, H.: The interpretation of microwave reflections from rainfall, J. Meteorol., 8, 271–282, 1951. 2399

Austin, P. M.: Relation between measured radar reflectivity and surface rainfall, Mon. Weather Rev., 115, 1053–1070, 1987. 2397

Azimi-Zonooz, A., Krajewski, W. F., Bowles, D. S., and Seo, D.-J.: Spatial rainfall estimation

by linear and non-linear co-kriging of radar-rainfall and raingage data, Stochastic Hydrol. Hydraul., 3, 51–67, 1989. 2390
Battan, L. J.: Radar observation of the atmosphere, The University of Chicago Press, Chicago, 324 pp, 1973. 2389, 2397, 2403
Beard, K. V.: Terminal velocity of cloud and precipitation drops aloft, J. Atmos. Sci., 33, 851–864, 1976. 2404
Berenguer, M., Corral, C., Sánchez-Diezma, R., and Sempere Torres, D.: Hydrological validation of a radar-based nowcasting technique, J. Hydrometeorol., 6, 532–549, 2005. 2389, 2391
Berne, A. and Uijlenhoet, R.: A stochastic model of range profiles of raindrop size distributions: Application to radar attenuation correction, Geophys. Res. Lett., 32, L10803, doi:10.1029/2004GL021899, 2005. 2396, 2399, 2400, 2407, 2408, 2409
Berne, A. and Uijlenhoet, R.: Quantitative analysis of X-band weather radar attenuation correction accuracy, Nat. Hazards Earth Syst. Sci., 6, 419–425, 2006. 2396, 2399, 2400, 2407, 2408, 2409
Berne, A., Delrieu, G., Creutin, J.-D., and Obled, C.: Temporal and spatial resolution of rainfall measurements required for urban hydrology, J. Hydrol., 299, 166–179, 2004. 2388, 2402
Berne, A., Delrieu, G., and Andrieu, H.: Estimating the vertical structure of intense Mediterranean precipitation using two X-band weather radar systems, J. Atmos. Oceanic Technol., 22, 1656–1675, 2005a. 2391, 2396
Berne, A., ten Heggeler, M., Uijlenhoet, R., Delobbe, M., Dierickx, P., and de Wit, M.: A preliminary investigation of radar rainfall estimation in the Ardennes region and a first hydrological application for the Ourthe catchment, Nat. Hazards Earth Syst. Sci., 5, 267–274, 2005b. 2389
Borga, M.: Accuracy of radar rainfall estimates for streamflow simulation, J. Hydrol., 267, 26–39, 2002. 2389
Bras, R. L. and Rodríguez-Iturbe, I.: Random Functions and Hydrology, Addison-Wesley, Reading, Massachusetts, 559 pp, 1985. 2400
CHO-TNO: Precipitation and measurements of precipitation, Proceedings and Informations 23, Committee for Hydrological Research (CHO), Netherlands Organization for Applied Scientific Research (TNO), 88 pp, 1977. 2389
Clift, G. A.: Use of radar in meteorology, Technical Note 181, World Meteorological Organization, Geneva, 90 pp, 1985. 2397

Collier, C. G.: Accuracy of rainfall estimates by radar, Part I: Calibration by telemetering raingauges, J. Hydrol., 83, 207–223, 1986a. 2390
Collier, C. G.: Accuracy of rainfall estimates by radar, Part II: Comparison with raingauge network, J. Hydrol., 83, 225–235, 1986b. 2390
Collier, C. G.: Applications of weather radar systems: A guide to uses of radar data in meteorology and hydrology, Ellis Horwood, Chichester, 294 pp, 1989. 2397
Collier, C. G.: The application of a continental-scale radar database to hydrological process parametrization within Atmospheric General Circulation Models, J. Hydrol., 142, 301–318, 1993. 2389
Collier, C. G. and Knowles, J. M.: Accuracy of rainfall estimates by radar, Part III: Application for short-term flood forecasting, J. Hydrol., 83, 237–249, 1986. 2390
Creutin, J.-D., Delrieu, G., and Lebel, T.: Rain measurement by raingage-radar combination: A geostatistical approach, J. Atmos. Oceanic Technol., 5, 102–115, 1988. 2390
Creutin, J.-D., Andrieu, H., and Faure, D.: Use of a weather radar for the hydrology of a mountainous area. Part II: Radar measurement validation, J. Hydrol., 193, 26–44, 1997. 2391, 2397
Delrieu, G., Bellon, A., and Creutin, J.-D.: Estimation de lames d'eau spatiales à l'aide de données de pluviomètres et de radar météorologique: Application au pas de temps journalier dans la région de Montréal, J. Hydrol., 98, 315–344, 1988. 2390
Delrieu, G., Caoudal, S., and Creutin, J.-D.: Feasibility of using mountain return for the correction of ground-based X-band weather radar data, J. Atmos. Oceanic Technol., 14, 368–385, 1997. 2406
Delrieu, G., Hücke, L., and Creutin, J.-D.: Attenuation in rain for X- and C-band weather radar systems: Sensitivity with respect to the drop size distribution, J. Appl. Meteorol., 38, 57–68, 1999. 2400, 2407, 2409, 2421
Delrieu, G., Ducrocq, V., Gaume, E., Nicol, J., Payrastre, O., Yates, E., Kirstetter, P.-E., Andrieu, H., Ayral, P.-A., Bouvier, C., Creutin, J.-D., Livet, M., Anquetin, S., Lang, M., Neppel, L., Obled, C., Parent-du-Châtelet, J., Saulnier, G.-M., Walpersdorf, A., and Wobrock, W.: The catastrophic flash-flood event of 8–9 September 2002 in the Gard region, France: A first case study for the Cévennes-Vivarais Mediterranean Hydrometeorological Observatory, J. Hydrometeorol., 6, 34–52, 2005. 2389, 2391
Doviak, R. J.: A survey of radar rain measurement techniques, J. Clim. Appl. Meteorol., 22, 832–849, 1983. 2397

Durden, S. L., Haddad, Z. S., Kitiyakara, A., and Li, F. K.: Effects of nonuniform beam filling on rainfall retrieval for the TRMM precipitation radar, J. Atmos. Oceanic Technol., 15, 635–646, 1998. 2395

Georgakakos, K. P., Carsteanu, A. A., Sturdevant, P. L., and Cramer, J. A.: Observation and analysis of midwestern rain rates, J. Appl. Meteorol., 33, 1433–1444, 1994. 2388

Habib, E., Krajewski, W. F., Nespor, V., and Kruger, A.: Numerical simulation studies of rain gage data correction due to wind effect, J. Geophys. Res. (D), 104, 19 723–19 733, 1999. 2388

Haddad, Z. S. and Rosenfeld, D.: Optimality of empirical Z–R relations, Quart. J. Roy. Meteorol. Soc., 123, 1283–1293, 1997. 2392

Hitschfeld, W. and Bordan, J.: Errors inherent in the radar measurement of rainfall at attenuating wavelengths, J. Meteorol., 11, 58–67, 1954. 2396, 2405, 2409

Illingworth, A. J., Blackman, T. M., and Goddard, J. W. F.: Improved rainfall estimates in convective storms using polarisation diversity radar, Hydrol. Earth Syst. Sci., 4, 555–563, 2000. 2393

Jameson, A. R.: A comparison of microwave techniques for measuring rainfall, J. Appl. Meteorol., 30, 32–54, 1991. 2397

Jameson, A. R. and Kostinski, A. B.: What is a raindrop size distribution?, Bull. Amer. Meteorol. Soc., 82, 1169–1177, 2001. 2392

Joss, J. and Waldvogel, A.: Precipitation measurement and hydrology, in: Radar in meteorology: Battan memorial and 40th anniversary conference on radar meteorology, edited by Atlas, D., pp. 577–606, American Meteorological Society, Boston, 1990. 2395, 2397

Krajewski, W. F.: Cokriging of radar-rainfall and rain gage data, J. Geophys. Res. (D), 92, 9571–9580, 1987. 2390

Le Cam, L.: A stochastic description of precipitation, in: Proceedings of the 4th Berkeley Symposium on Mathematical Statistics and Probability, volume IV, edited by Neyman, J., pp. 165–186, University of California, Berkeley, 1961. 2388

Lovejoy, S. and Schertzer, D.: Fractals, raindrops and resolution dependence of rain measurements, J. Appl. Meteorol., 29, 1167–1170, 1990a. 2388

Lovejoy, S. and Schertzer, D.: Multifractals, universality classes and satellite and radar measurements of cloud and rain fields, J. Geophys. Res. (D), 95, 2021–2034, 1990b. 2388

Lovejoy, S. and Schertzer, D.: Multifractals and rain, in: New Uncertainty Concepts in Hydrology and Water Resources, edited by Kundzewicz, Z. W., pp. 61–103, Cambridge University

Press, Cambridge, 1995. 2388
Marshall, J. S. and Palmer, W. M.: The distribution of raindrops with size, J. Meteorol., 5, 165–166, 1948. 2392
Marzoug, M. and Amayenc, P.: A class of single- and dual-frequency algorithms for rain-rate profiling from a spaceborne radar. Part I: Principle and tests from numerical simulations, J. Atmos. Oceanic Technol., 11, 1480–1506, 1994. 2396, 2406
Neff, E. L.: How much rain does a rain gage gage?, J. Hydrol., 35, 213–220, 1977. 2388
Ogden, F. L., Richardson, J. R., Smith, J. A., and Smith, M. E.: Fort Collins flood data set created, EOS Trans. Amer. Geophys. Union, 80, 257–258, 1999. 2389
Pamment, J. A. and Conway, B. J.: Objective identification of echoes due to anomalous propagation in weather radar data, J. Atmos. Oceanic Technol., 15, 98–113, 1998. 2397
Rodríguez-Iturbe, I.: Scale of fluctuation of rainfall models, Water Resour. Res., 22, 15S–37S, 1986. 2388
Rodríguez-Iturbe, I.: Exploring complexity in the structure of rainfall, Adv. Water Resour., 14, 162–167, 1991. 2388
Rodríguez-Iturbe, I. and Eagleson, P. S.: Mathematical models of rainstorm events in space and time, Water Resour. Res., 23, 181–190, 1987. 2388
Rodríguez-Iturbe, I., Gupta, V. K., and Waymire, E.: Scale considerations in the modeling of temporal rainfall, Water Resour. Res., 20, 1611–1619, 1984. 2388
Rodríguez-Iturbe, I., Cox, D. R., and Eagleson, P. S.: Spatial modelling of total storm rainfall, Proc. R. Soc. Lond., A 403, 27–50, 1986. 2388
Rodríguez-Iturbe, I., Cox, D. R., and Isham, V.: Some models for rainfall based on stochastic point processes, Proc. R. Soc. Lond., A 410, 269–288, 1987. 2388
Rodríguez-Iturbe, I., Cox, D. R., and Isham, V.: A point process model for rainfall: Further developments, Proc. R. Soc. Lond., A 417, 283–298, 1988. 2388
Rodríguez-Iturbe, I., Febres de Power, B., Sharifi, M. B., and Georgakakos, K. P.: Chaos in rainfall, Water Resour. Res., 25, 1667–1675, 1989. 2388
Sánchez-Diezma, R., Zawadzki, I., and Sempere Torres, D.: Identification of the bright band through the analysis of volumetric radar data, J. Geophys. Res. (D), 105, 2225–2236, 2000. 2391, 2396
Sánchez-Diezma, R., Sempere Torres, D., Creutin, J.-D., Zawadzki, I., and Delrieu, G.: Factors affecting the precision of radar measurement of rain: Assessment from an hydrological perspective, in: Preprints of the 30th International Conference on Radar Meteorology, pp.

573–575, American Meteorological Society, Boston, 2001. 2397
Sauvageot, H.: Radarmétéorologie. Télédétection active de l'atmosphère, Eyrolles / CNET-ENST, Paris, 296 pp, 1982. 2397
Sempere Torres, D., Corral, C., Raso, J., and Malgrat, P.: Use of weather radar for combined sewer overflows monitoring and control, J. Environ. Eng., 125, 372–380, 1999. 2389
Seo, D.-J. and Smith, J. A.: Rainfall estimation using raingages and radar – a Bayesian approach: 1. Derivation of estimators, Stochastic Hydrol. Hydraul., 5, 17–29, 1991a. 2390
Seo, D.-J. and Smith, J. A.: Rainfall estimation using raingages and radar – a Bayesian approach: 2. An application, Stochastic Hydrol. Hydraul., 5, 31–44, 1991b. 2390
Seo, D.-J., Krajewski, W. F., and Bowles, D. S.: Stochastic interpolation of rainfall data from rain gages and radar using cokriging. 1. Design of experiments, Water Resour. Res., 26, 469–477, 1990a. 2390
Seo, D.-J., Krajewski, W. F., Azimi-Zonooz, A., and Bowles, D. S.: Stochastic interpolation of rainfall data from rain gages and radar using cokriging. 2. Results, Water Resour. Res., 26, 915–924, 1990b. 2390
Serrar, S., Delrieu, G., Creutin, J.-D., and Uijlenhoet, R.: Mountain reference technique: Use of mountain returns to calibrate weather radars operating at attenuating wavelengths, J. Geophys. Res. (D), 105, 2281–2290, 2000. 2391, 2397
Sevruk, B.: Reliability of precipitation measurement, in: Precipitation Measurement, edited by Sevruk, B., pp. 13–19, Swiss Federal Institute of Technology (ETH), Zurich, 1989. 2388
Smith, J. A.: Statistical modeling of daily rainfall occurrences, Water Resour. Res., 23, 885–893, 1987. 2388
Smith, J. A.: Precipitation, in: Handbook of Hydrology, edited by Maidment, D. R., pp. 3.1–3.47, McGraw-Hill, New York, 1993. 2390
Smith, J. A. and Karr, A. F.: A point process model of summer season rainfall occurrences, Water Resour. Res., 19, 95–103, 1983. 2388
Smith, J. A. and Karr, A. F.: Parameter estimation for a model of space-time rainfall, Water Resour. Res., 21, 1251–1257, 1985. 2388
Smith, J. A. and Krajewski, W. F.: A modeling study of rainfall rate-reflectivity relationships, Water Resour. Res., 29, 2505–2514, 1993. 2391
Smith, J. A., Seo, D.-J., Baeck, M. L., and Hudlow, M. D.: An intercomparison study of NEXRAD precipitation estimates, Water Resour. Res., 32, 2035–2045, 1996a. 2391
Smith, J. A., Baeck, M. L., Steiner, M., and Miller, A. J.: Catastrophic rainfall from an upslope

thunderstorm in the central Appalachians: The Rapidan storm of June 27, 1995, Water Resour. Res., 32, 3099–3113, 1996b. 2389, 2391
Steiner, M., Smith, J. A., Burges, S. J., Alonso, C. V., and Darden, R. W.: Effect of bias adjustment and rain gauge data quality control on radar rainfall estimation, Water Resour. Res., 35, 2487–2503, 1999. 2388
Testud, J., Le Bouar, E., Obligis, E., and Ali-Mehenni, M.: The rain profiling algorithm applied to polarimetric weather radar, J. Atmos. Oceanic Technol., 17, 332–356, 2000. 2393
Uijlenhoet, R.: Raindrop size distributions and radar reflectivity-rain rate relationships for radar hydrology, Hydrol. Earth Syst. Sci., 5, 615–627, 2001. 2392, 2403
Uijlenhoet, R. and Sempere Torres, D.: Measurement and parameterization of rainfall microstructure, J. Hydrol., 328, 1–7, doi:10.1016/j.jhydrol.2005.11.038, 2006. 2392
Uijlenhoet, R. and Stricker, J. N. M.: A consistent rainfall parameterization based on the exponential raindrop size distribution, J. Hydrol., 218, 101–127, 1999. 2392
Uijlenhoet, R., Andrieu, H., Austin, G. L., Baltas, E., Borga, M., Brilly, M., Cluckie, I. D., Creutin, J.-D., Delrieu, G., Deshons, P., Fattorelli, S., Griffith, R. J., Guarnieri, P., Han, D., Mimikou, M., Monai, M., Porrà, J. M., Sempere Torres, D., and Spagni, D. A.: HYDROMET Integrated Radar Experiment (HIRE): Experimental setup and first results, in: Preprints of the 29th International Conference on Radar Meteorology, pp. 926–930, American Meteorological Society, Boston, 1999a. 2402
Uijlenhoet, R., Stricker, J. N. M., Torfs, P. J. J. F., and Creutin, J.-D.: Towards a stochastic model of rainfall for radar hydrology: Testing the Poisson homogeneity hypothesis, Phys. Chem. Earth (B), 24, 747–755, 1999b. 2392
van de Hulst, H. C.: Light scattering by small particles, Dover, New York, 470 pp, 1981. 2404
Vanmarcke, E.: Random fields: Analysis and synthesis, The MIT Press, Cambridge, Massachusetts, 382 pp, 1983. 2401
Veneziano, D., Langousis, A., and Furcolo, P.: Multifractality and rainfall extremes: A review, Water Resour. Res., 42, W06D15, doi:10.1029/2005WR004716, 2006. 2388
Venugopal, V., Roux, S. G., Foufoula-Georgiou, E., and Arneodo, A.: Revisiting multifractality of high-resolution temporal rainfall using a wavelet-based formalism, Water Resour. Res., 42, W06D14, doi:10.1029/2005WR004489, 2006. 2388
Vulpiani, G., Marzano, F. S., Chandrasekar, V., and Uijlenhoet, R.: Model-based iterative approach to polarimetric radar rainfall estimation in presence of path attenuation, Adv. Geosci., 2, 51–57, 2005. 2393

Vulpiani, G., Marzano, F. S., Chandrasekar, V., Berne, A., and Uijlenhoet, R.: Rainfall rate retrieval in presence of path attenuation using C-band polarimetric weather radars, Nat. Hazards Earth Syst. Sci., 6, 439–450, 2006. 2393

Waymire, E. and Gupta, V. K.: The mathematical structure of rainfall representations 1. A review of the stochastic rainfall models, Water Resour. Res., 17, 1261–1272, 1981a. 2388

Waymire, E. and Gupta, V. K.: The mathematical structure of rainfall representations 2. A review of the theory of point processes, Water Resour. Res., 17, 1273–1285, 1981b. 2388

Waymire, E. and Gupta, V. K.: The mathematical structure of rainfall representations 3. Some applications of the point process theory to rainfall processes, Water Resour. Res., 17, 1287–1294, 1981c. 2388

Waymire, E., Gupta, V. K., and Rodríguez-Iturbe, I.: A spectral theory of rainfall intensity at the meso-β scale, Water Resour. Res., 20, 1453–1465, 1984. 2388

Wilson, J. W. and Brandes, E. A.: Radar measurement of rainfall – A summary, Bull. Amer. Meteorol. Soc., 60, 1048–1058, 1979. 2392, 2397

Wood, S. J., Jones, D. A., and Moore, R. J.: Accuracy of rainfall measurement for scales of hydrological interest, Hydrol. Earth Syst. Sci., 4, 531–541, 2000. 2388

Zawadzki, I.: Factors affecting the precision of radar measurements of rain, in: Preprints of the 22nd Conference on Radar Meteorology, pp. 251–256, American Meteorological Society, Boston, 1984. 2397

Table 1. Mean, standard deviation and scale of fluctuation [km] of $N' = \ln N_t$ (with N_t in m^{-3}) and $\Lambda' = \ln \Lambda$ (with Λ in mm^{-1}) deduced from HIRE'98 data (07/09/1998 event) for moderate (4-s time step) and intense (2-s time step) rainfall parameterization.

		Mean	Std	θ
N'	moderate	7.85	0.43	6.3
	intense	8.11	0.41	4.4
Λ'	moderate	1.08	0.19	6.3
	intense	0.93	0.31	4.4

Table 2. Path-average radar reflectivity Z [$mm^6\,m^{-3}$], rain rate R [$mm\,h^{-1}$], and specific attenuation k [$dB\,km^{-1}$] for moderate and intense rainfall parameterization for different weather radar frequency bands (X-, C-, and S-band). Values between brackets indicate coefficient of variation (ratio of standard deviation and mean) at 500 m resolution.

	moderate rainfall		
	Z	R	k
X-band	38.8 (0.056)	9.43 (0.29)	0.121 (0.41)
C-band	37.6 (0.049)	9.39 (0.28)	0.017 (0.36)
S-band	38.0 (0.048)	9.46 (0.28)	0.003 (0.27)
	intense rainfall		
	Z	R	k
X-band	47.7 (0.075)	28.5 (0.46)	0.594 (0.64)
C-band	45.6 (0.077)	28.1 (0.47)	0.100 (0.81)
S-band	45.4 (0.070)	28.2 (0.48)	0.010 (0.54)

Table 3. Climatological Z–R and Z–k relations (with Z in $\mathrm{mm^6\,m^{-3}}$, R in $\mathrm{mm\,h^{-1}}$, and k in $\mathrm{dB\,km^{-1}}$) at X-, C-, and S-band, estimated following the procedure outlined by Delrieu et al. (1999), using a large dataset of DSD measurements collected in southern France.

	Z–R	Z–k
X-band (3.2 cm)	$Z=233\,R^{1.59}$	$Z=1.18\times10^{5}\,k^{1.26}$
C-band (5.6 cm)	$Z=256\,R^{1.45}$	$Z=6.57\times10^{5}\,k^{1.11}$
S-band (10.0 cm)	$Z=311\,R^{1.40}$	$Z=1.70\times10^{7}\,k^{1.33}$

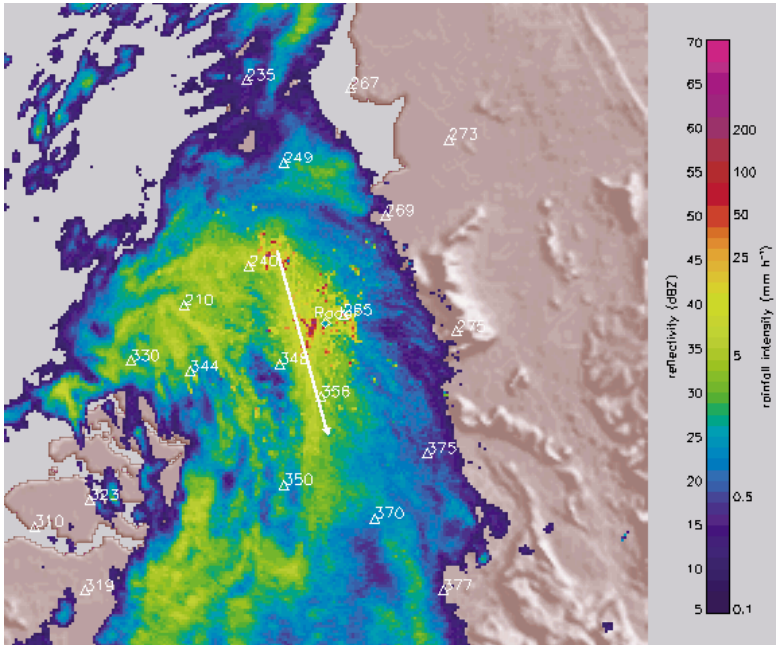

Fig. 1. Plan Position Indicator or PPI of the lowest elevation of the KNMI C-band weather radar at De Bilt at 11:47 a.m. on 19 September 2001, projected on a map of The Netherlands, showing reflectivities [dBZ] and rain rates [mm h^{-1}] derived using the Marshall-Palmer Z–R relationship. Included are 32 rain gauge locations, the radar site and a straight line representing the location of the vertical cross section (a so-called "Range Height Indicator", or RHI) which is visualized in Fig. 8. The strong reflectivities are considered to be ground clutter because of their location and temporal invariability (this PPI was constructed with the radar data visualization software VISRAD of the Group of Applied Research on Hydrometeorology, Technical University of Catalonia, UPC, Barcelona, Spain).

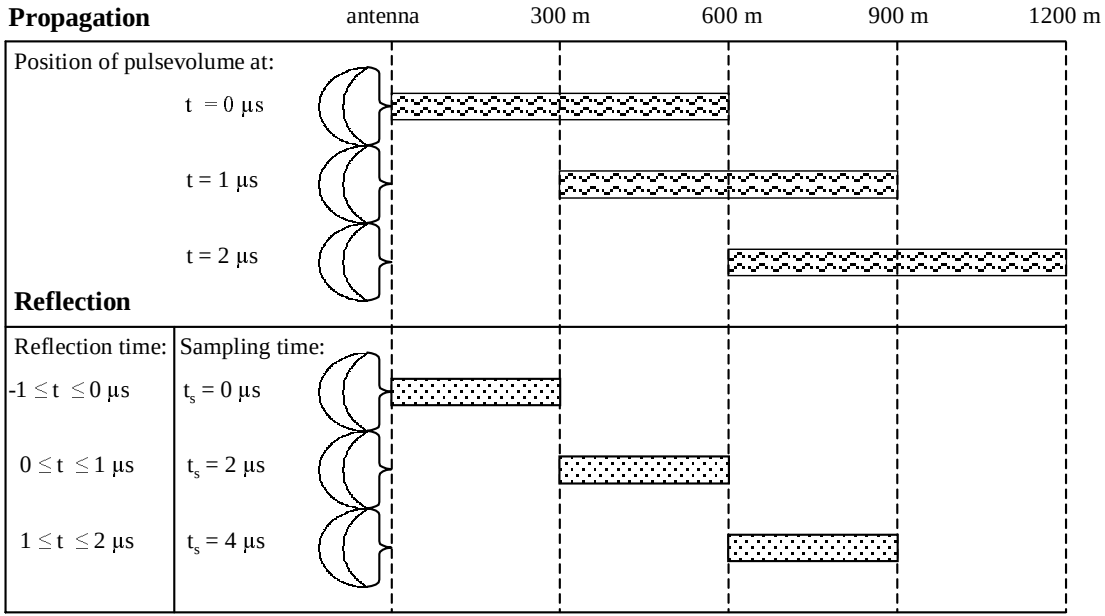

Fig. 2. The propagation of a pulse volume (corresponding to the transmitted signal) and the associated sample volume (corresponding to the backscattered signal received at a certain sampling moment) with respect to the radar antenna.

HESSD
3, 2385–2436, 2006

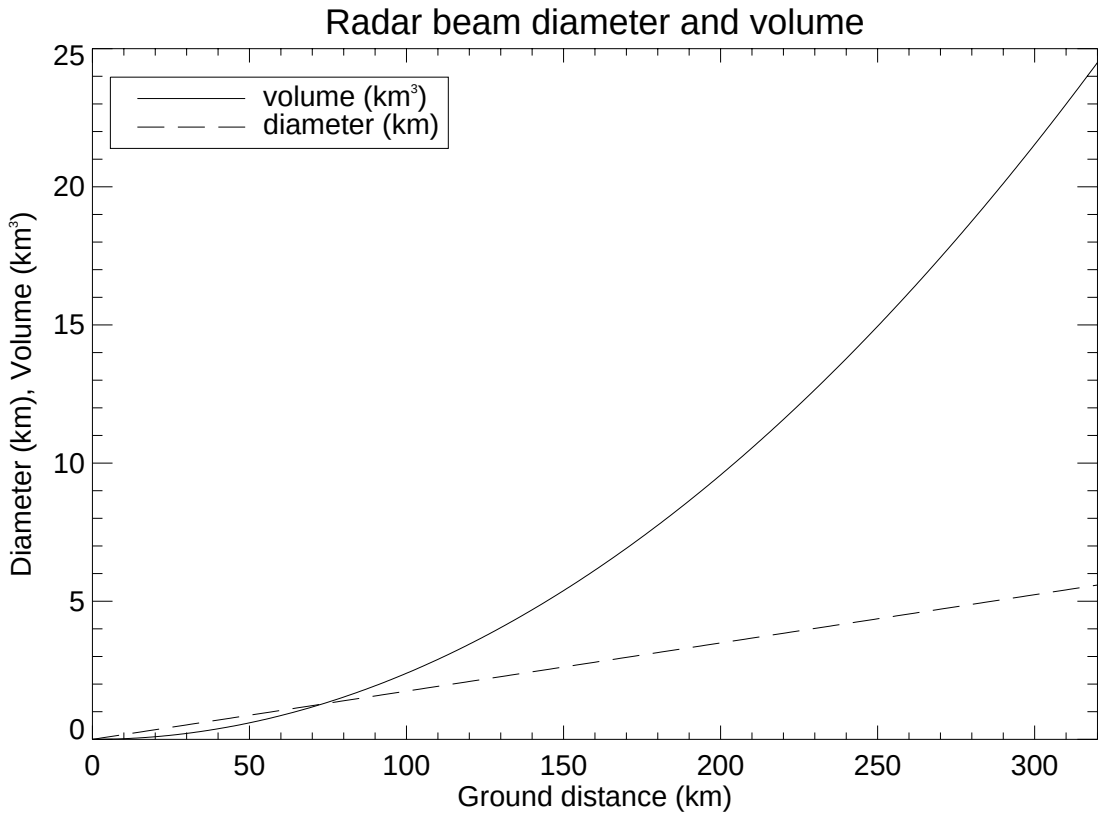

Fig. 3. Range dependence of the diameter and sample volume of the KNMI radar, assuming the radar sample volume is limited by its half-power beam width (Fig. 4).

HESSD
3, 2385–2436, 2006

EGU

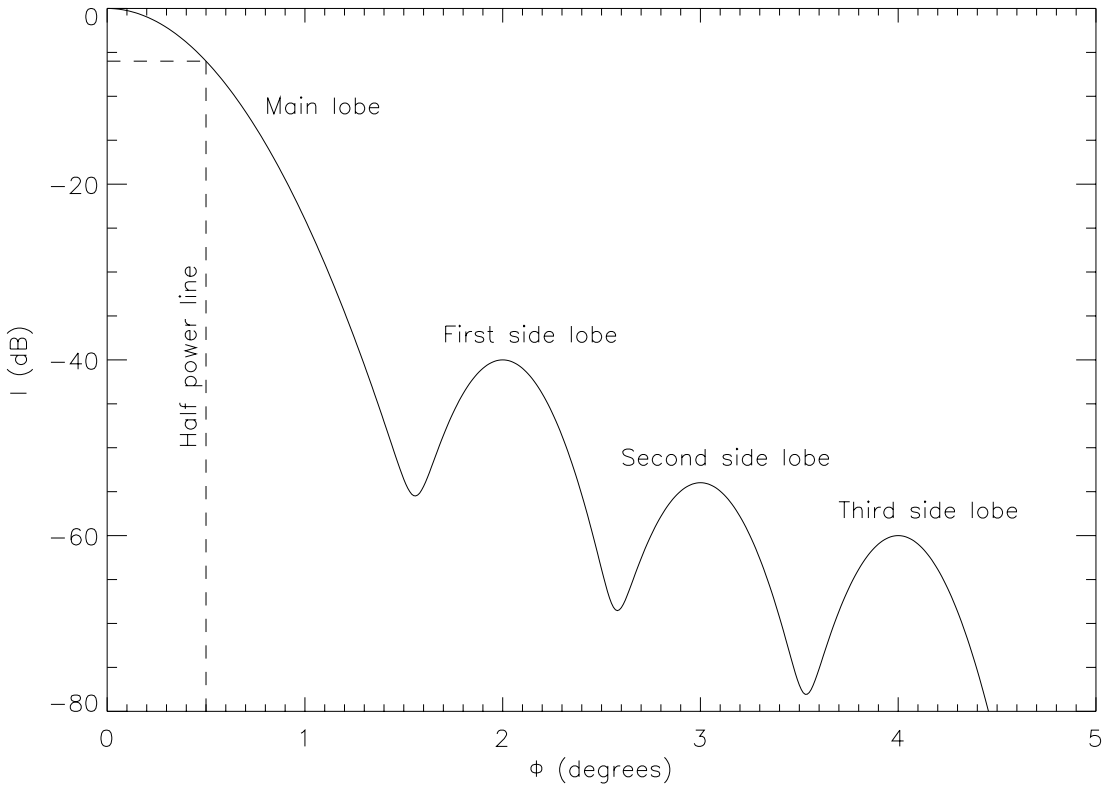

Fig. 4. Theoretical two-way gain function of an antenna having a half-power beam width of 1.0°, where *I* is the distribution of power in each side lobe with respect to the power in the main lobe in decibels.

HESSD
3, 2385–2436, 2006

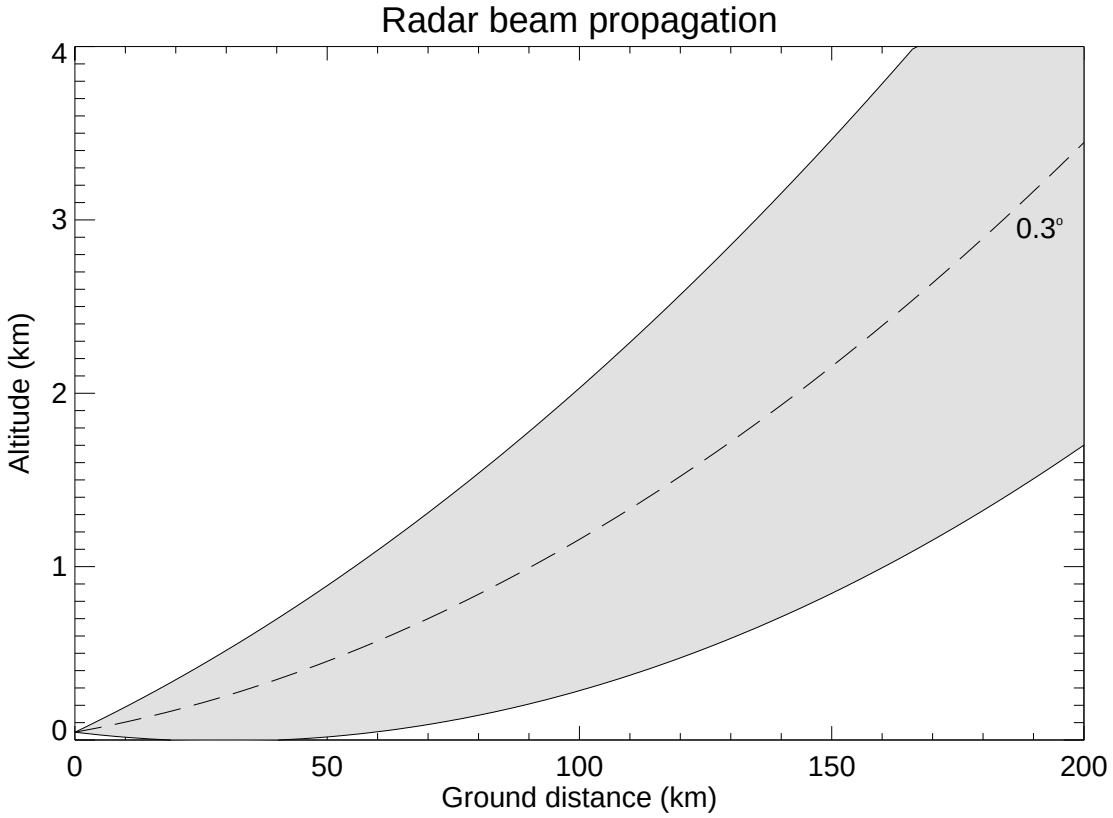

Fig. 5. Propagation of the KNMI radar beam at its lowest elevation angle of 0.3°. The solid lines represent the half-power beam width and the dashed line the center of the beam.

HESSD
3, 2385–2436, 2006

EGU

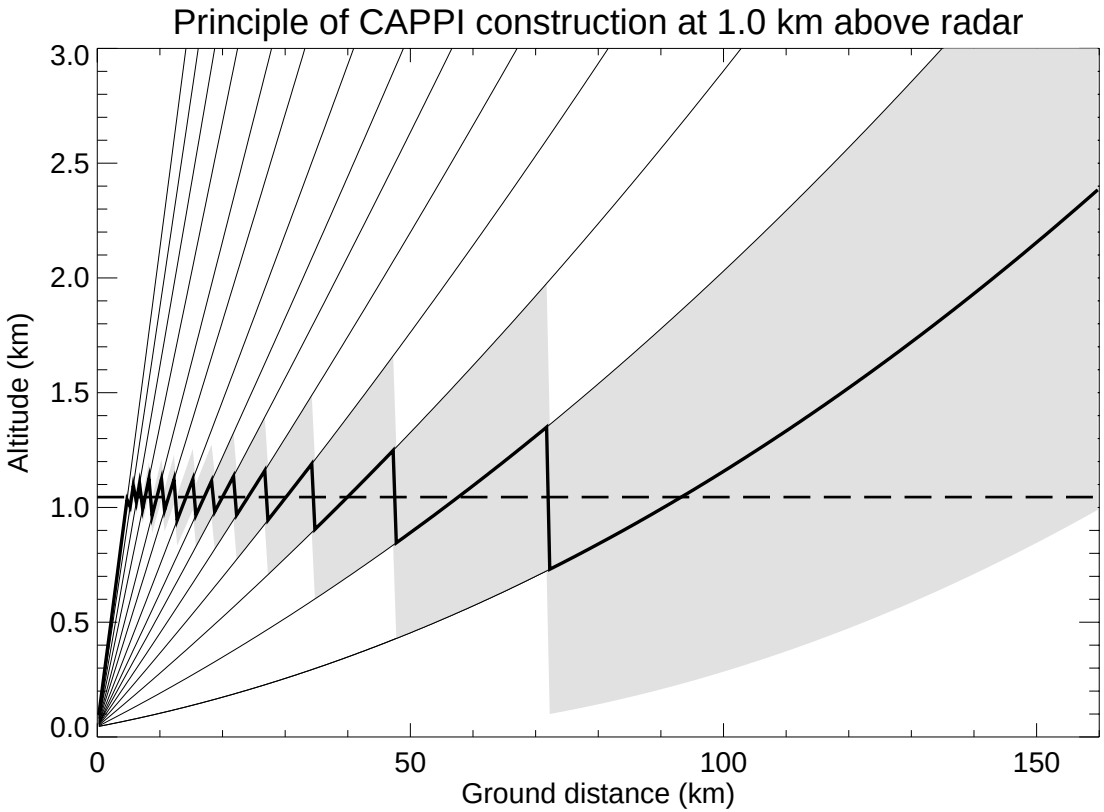

Fig. 6. Construction principle of a CAPPI for the KNMI radar, using all 14 elevation angles. The dashed line represents a pseudo-CAPPI height of about 1 km above the radar. The solid bold line represents the centers of the beams closest to the selected CAPPI height at a particular distance from the radar. The gray area represents the half-power sampling volume of the beams concerned.

HESSD
3, 2385–2436, 2006

EGU

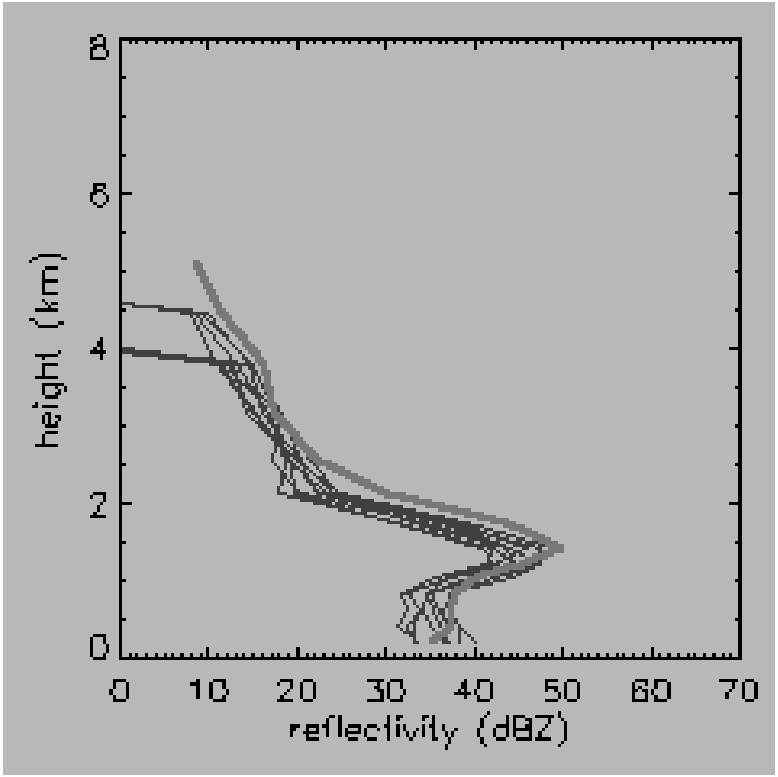

Fig. 7. Vertical profile of reflectivity (VPR) [dBZ], clearly showing a bright band at an altitude of approximately 1.5 km. The bold gray line is the VPR in a certain radar pixel, whereas the thin lines are the VPRs in the surrounding pixels (the profiles were constructed in VISRAD).

HESSD
3, 2385–2436, 2006

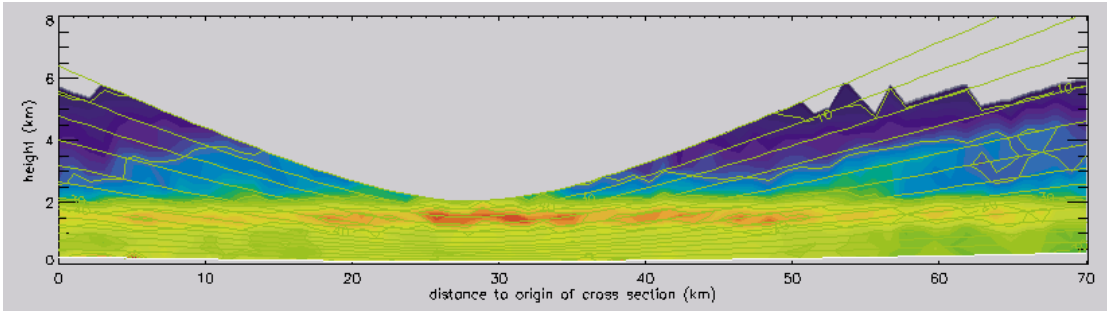

Fig. 8. Range Height Indicator (RHI) of measured reflectivities, clearly showing a bright band at an altitude of approximately 1.5 km (constructed in VISRAD). The corresponding location, date, time and rainfall rates can be found in Fig. 1.

Fig. 9. The locations of the KNMI radar site (△) and the automatic KNMI rain gauges (∗) in The Netherlands. Concentric circles around the radar antenna with a radius of 50 and 100 km give an indication of the distance of the gauges to the radar site.

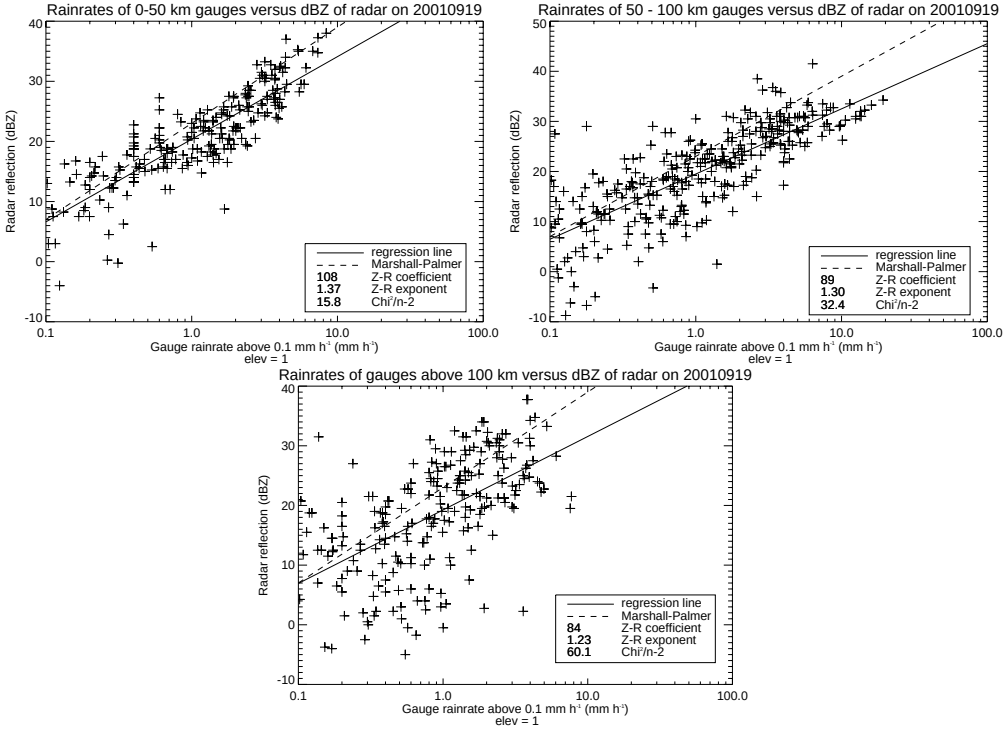

Fig. 10. Empirical Z–R relations for different range intervals. Measured (radar-gauge pairs, +) and fitted relations (solid lines), compared to the Marshall-Palmer law (dashed lines). Upper panel: 0–50 km; Middle panel: 50–100 km; Lower panel: >100 km.

HESSD
3, 2385–2436, 2006

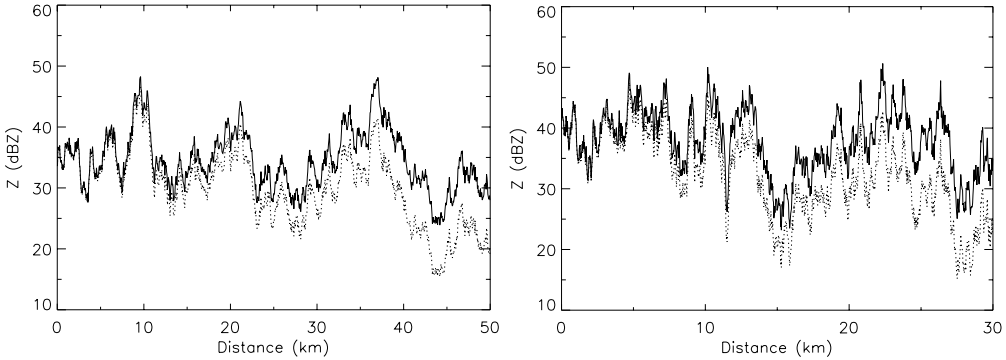

Fig. 11. Examples of non-attenuated (Z, solid) and attenuated (Z_A, dashed) radar reflectivity profiles at X-band for moderate (top panel) and intense (bottom panel) rainfall parameterizations. Reflectivities are expressed on a logarithmic (decibel) scale, where dBZ=10 log(Z).

HESSD
3, 2385–2436, 2006

EGU

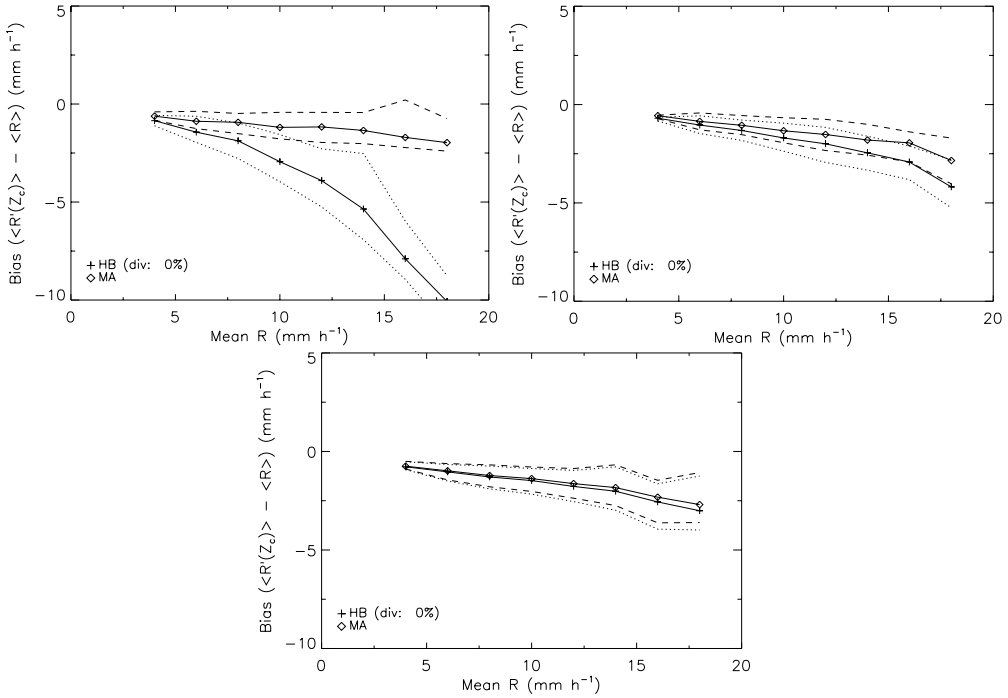

Fig. 12. Median (solid line), 10%, and 90% quantiles (dotted and dashed lines) of the distribution of the mean bias error (MBE) between the retrieved ($R'(Z_c)$, where Z_c denotes attenuation-corrected Z) and the actual (R) rain rate profiles as a function of the path-average rain rate for 1000 profiles of 50 km length at 500 m resolution for the moderate rainfall parameterization. "HB" indicates the Hitschfeld-Bordan (forward) attenuation correction algorithm ("div" indicates the percentage of diverging corrections) and "MA" indicates the Marzoug-Amayenc (backward) algorithm. Upper panel: X-band; Middle panel: C-band; Lower panel: S-band.

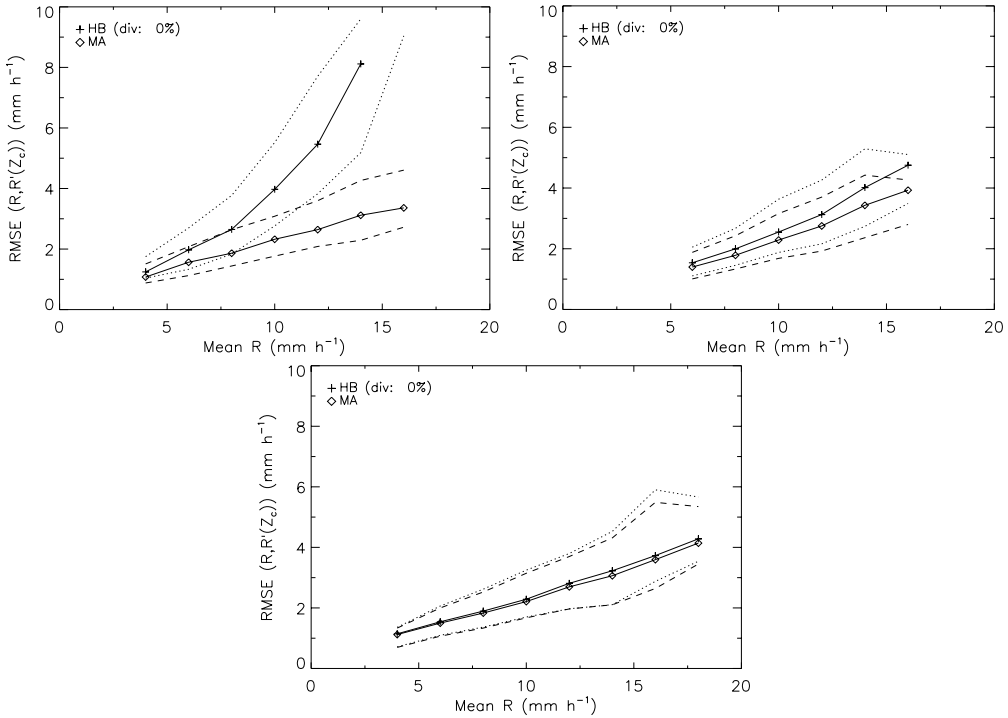

Fig. 13. Median (solid line), 10%, and 90% quantiles (dotted and dashed lines) of the distribution of the root mean square error (RMSE) between the retrieved ($R'(Z_c)$, where Z_c denotes attenuation-corrected Z) and the actual (R) rain rate profiles as a function of the path-average rain rate for 1000 profiles of 50 km length at 500 m resolution for the moderate rainfall parameterization. "HB" indicates the Hitschfeld-Bordan (forward) attenuation correction algorithm ("div" indicates the percentage of diverging corrections) and "MA" indicates the Marzoug-Amayenc (backward) algorithm. Upper panel: X-band; Middle panel: C-band; Lower panel: S-band.

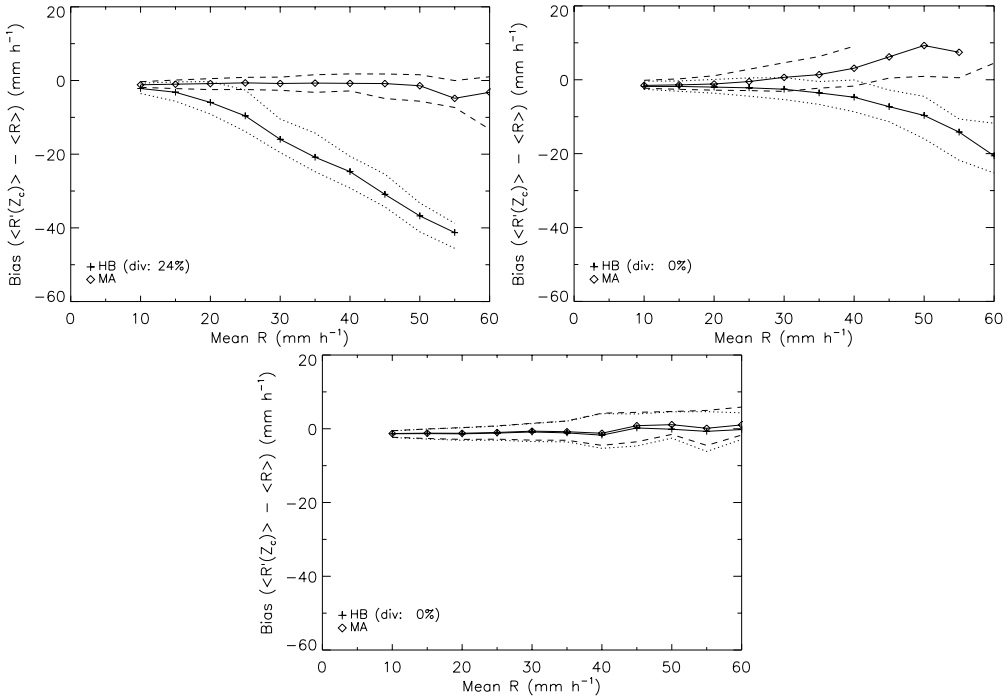

Fig. 14. Median (solid line), 10%, and 90% quantiles (dotted and dashed lines) of the distribution of the mean bias error (MBE) between the retrieved ($R'(Z_c)$, where Z_c denotes attenuation-corrected Z) and the actual (R) rain rate profiles as a function of the path-average rain rate for 1000 profiles of 30 km length at 500 m resolution for the intense rainfall parameterization. "HB" indicates the Hitschfeld-Bordan (forward) attenuation correction algorithm ("div" indicates the percentage of diverging corrections) and "MA" indicates the Marzoug-Amayenc (backward) algorithm. Upper panel: X-band; Middle panel: C-band; Lower panel: S-band.

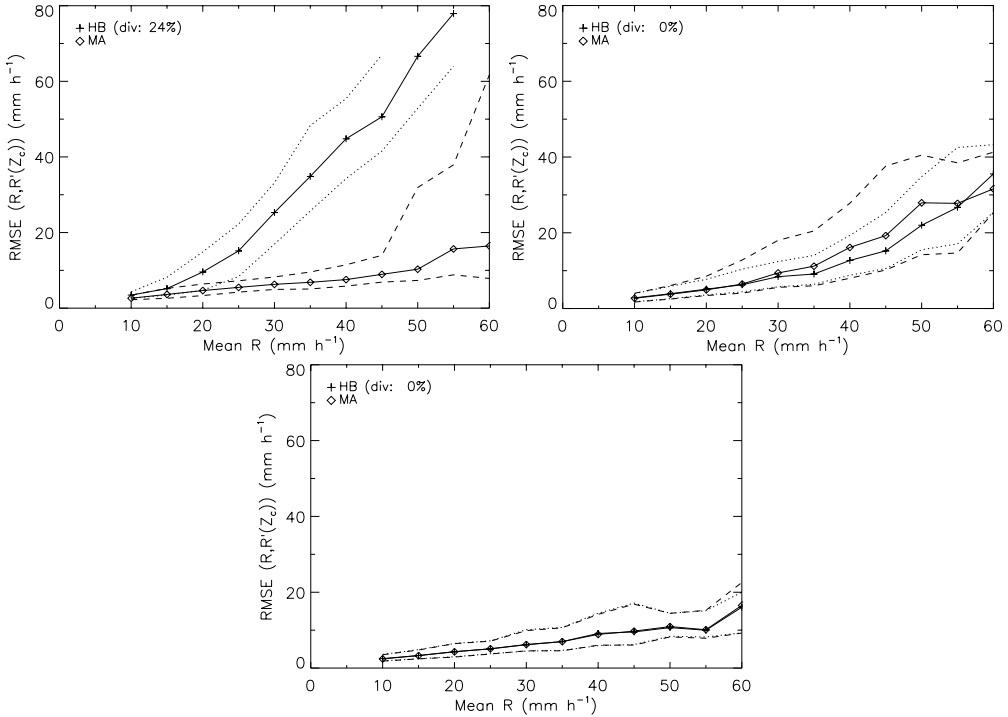

Fig. 15. Median (solid line), 10%, and 90% quantiles (dotted and dashed lines) of the distribution of the root mean square error (RMSE) between the retrieved ($R'(Z_c)$, where Z_c denotes attenuation-corrected Z) and the actual (R) rain rate profiles as a function of the path-average rain rate for 1000 profiles of 30 km length at 500 m resolution for the intense rainfall parameterization. "HB" indicates the Hitschfeld-Bordan (forward) attenuation correction algorithm ("div" indicates the percentage of diverging corrections) and "MA" indicates the Marzoug-Amayenc (backward) algorithm. Upper panel: X-band; Middle panel: C-band; Lower panel: S-band.